Acta Pharmaceutica Sinica B 2022;12(4):1899–1912

Chinese Pharmaceutical Association
Institute of Materia Medica, Chinese Academy of Medical Sciences

Acta Pharmaceutica Sinica B

www.elsevier.com/locate/apsb
www.sciencedirect.com

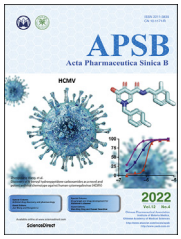

ORIGINAL ARTICLE

Disruption of adipocyte HIF-1α improves atherosclerosis through the inhibition of ceramide generation

Pengcheng Wang[a,b,d,†], Guangyi Zeng[a,b,d,†], Yu Yan[a,d], Song-yang Zhang[a,d], Yongqiang Dong[a,d], Yangming Zhang[a,d], Xingzhong Zhang[a,d], Huiying Liu[a,d], Zhipeng Zhang[e], Changtao Jiang[a,b,d,*], Yanli Pang[c,*]

[a]*Department of Physiology and Pathophysiology, School of Basic Medical Sciences, Peking University, Key Laboratory of Molecular Cardiovascular Science, Ministry of Education, Beijing 100191, China*
[b]*Center of Basic Medical Research, Institute of Medical Innovation and Research, Peking University Third Hospital, Beijing 100191 China*
[c]*Center for Reproductive Medicine, Department of Obstetrics and Gynecology, Peking University Third Hospital, Beijing 100191 China*
[d]*Center for Obesity and Metabolic Disease Research, School of Basic Medical Sciences, Peking University, Beijing 100191, China*
[e]*General Surgery Department, Peking University Third Hospital, Beijing 100191, China*

Received 12 July 2021; received in revised form 5 September 2021; accepted 14 September 2021

KEY WORDS
HIF-1α;

Abstract Atherosclerosis is a chronic multifactorial cardiovascular disease. Western diets have been reported to affect atherosclerosis through regulating adipose function. In high cholesterol diet-fed

Abbreviations: HIF-1α/2α/3α, hypoxia-inducible factor 1 alpha/2 alpha/3 alpha; APOE, apolipoprotein E; PLS-DA, partial least squares discriminant analysis; VIP, variable importance for the projection; eWAT, epididymal white adipose tissue; SM, sphingomyelin; PC, phosphatidylcholine; SMase, sphingomyelinase; VLDL, very low-density lipoprotein; LDL, low-density lipoprotein; HDL, high-density lipoprotein; MCP-1, monocyte chemoattractant protein-1; TNF-α, tumor necrosis factor alpha; IL-6/1β, interleukin-6/1β; MAC-2, lectin, galactose binding, soluble 3; CXCL1, chemokine (C−X−C motif) ligand 1 protein; CCL5, chemokine (C−C motif) ligand 5; VEGF, vascular endothelial growth factor; SPTLC1/2/3, serine palmitoyltransferase long chain base subunit 1/2/3; DEGS1, delta(4)-desaturase, sphingolipid 1; SGMS1, sphingomyelin synthase 1; CERS2/4/5/6, ceramide synthase 2/4/5/6; SMPD1/2/3/4, sphingomyelin phosphodiesterase 1/2/3/4; ACER2/3, alkaline ceramidase 2/3; EIF5, eukaryotic translation initiation factor 5; ARNT, aryl hydrocarbon nuclear translocator; HREs, HIF-response elements; ChIP, chromatin immunoprecipitation; $CoCl_2$, cobalt(II) chloride; GFP, green fluorescent protein.

*Corresponding authors.
E-mail addresses: jiangchangtao@bjmu.edu.cn (Changtao Jiang), yanlipang@bjmu.edu.cn (Yanli Pang).

†These authors made equal contributions in this work.

Peer review under responsibility of Chinese Pharmaceutical Association and Institute of Materia Medica, Chinese Academy of Medical Sciences.

https://doi.org/10.1016/j.apsb.2021.10.001

SMPD3;
Ceramide;
PX-478;
Adipocyte;
Cholesterol;
Inflammatory responses;
Atherosclerosis

ApoE$^{-/-}$ mice, adipocyte HIF-1α deficiency or direct inhibition of HIF-1α by the selective pharmacological HIF-1α inhibitor PX-478 alleviates high cholesterol diet-induced atherosclerosis by reducing adipose ceramide generation, which lowers cholesterol levels and reduces inflammatory responses, resulting in improved dyslipidemia and atherogenesis. *Smpd3*, the gene encoding neutral sphingomyelinase, is identified as a new target gene directly regulated by HIF-1α that is involved in ceramide generation. Injection of lentivirus-SMPD3 in epididymal adipose tissue reverses the decrease in ceramides in adipocytes and eliminates the improvements on atherosclerosis in the adipocyte HIF-1α-deficient mice. Therefore, HIF-1α inhibition may constitute a novel approach to slow atherosclerotic progression.

1. Introduction

Atherosclerosis is a universal problem in modern society that remains the leading cause of mortality worldwide[1−3]. The pathogenesis of atherosclerosis is caused by a combination of risk factors, of which dyslipidemia is a major risk factor for atherosclerotic cardiovascular disease[4,5]. Excessively expanded adipocytes and accumulated lipids cause obesity, which in turn leads to adipose tissue dysfunction[6,7]. Importantly, as an energy storage organ, adipose tissue is also an endocrine organ, secreting adipocytokines that affect the function of cells and tissues throughout the body[8]. Impaired lipid metabolism, such as elevated low-density lipoprotein (LDL) cholesterol, is the basis of atherosclerotic lesions[2,9−11]. Changes in lipid components of adipose tissues have profound effects on inflammatory responses, which promotes atherosclerosis[12,13]. However, repairing dysfunctional adipose tissue can improve systemic metabolic balance, thus decreasing atherosclerosis in mice[14]. Therefore, targeting metabolic pathways in adipose tissue has become a potential treatment for atherosclerosis.

In the development of obesity, the underdeveloped vasculature cannot keep up with the expansion of adipose tissue, which leads to local hypoxia and activates hypoxia-inducible factors (HIFs)[15,16]. HIF is a heterodimer that consisting of one alpha subunit bound to the aryl hydrocarbon nuclear translocator (ARNT, also known as HIF-1β). HIF-α subunits contain three subtypes: HIF-1α, HIF-2α, and HIF-3α[17]. During hypoxia, HIF-α avoids hydroxylation, ubiquitination and proteasome-mediated degradation, and dimerizes with HIF-1β to activate target genes such as vascular endothelial growth factor (VEGF), glucose transporters and glycolytic enzymes[18−20], through combining with the hypoxia response elements (HRE). Obesity-associated adipose hypoxia triggers increased expression of HIF-1α, which promotes the disease process. Overexpression of HIF-1α initiates adipose tissue fibrosis and induces adipocyte chemokine production with increased tissue inflammation, which results in glucose intolerance and insulin resistance[21,22]. Genetic or pharmacologic inhibition of HIF-1α can prevent or reverse the associated pathophysiological processes[23−25]. However, the role of adipose HIF-1α and the exact mechanisms in atherosclerosis are still unclear.

Ceramides, the main phospholipids for biofilm components, are important second messengers[26] involved in cell growth inhibition and apoptosis, and interact with several pathways to promote insulin resistance, oxidative stress and inflammation, which are all linked to atherosclerosis[27,28]. In preclinical studies of obesity, ceramides are considered as toxic lipids, and abnormal accumulation of ceramides is a putative intermediate link between excess adiposity and metabolic diseases[29]. Notably, inhibiting the biosynthetic process or increasing the degradation of ceramides ameliorated metabolic disorders, including insulin resistance, atherosclerosis and steatohepatitis, in rodents[28,30].

Visceral adipose tissue is one of the major sources for ceramide synthesis[31]. Ceramides are generally synthesized by three pathways *in vivo*[26], of which the sphingomyelinase (SMase) pathway has been reported to be involved in the pathogenesis of atherogenesis[32]. Type 2-neutral SMase (nSMase2, also called SMPD3), located in membrane structures by lipid bilayer insertion of palmitoylated residues and interaction with anionic phospholipid, catalyzes the hydrolysis of sphingomyelin to form ceramide and phosphocholine[33]. Activation of SMPD3 by oxidized LDLs (oxLDLs), TNF-α, IL-1β, IFN-γ, and oxidative stress may contribute to endothelial activation and inflammation[34,35]. Consequently, SMPD3 deficiency or the use of the specific inhibitor GW4869 inhibited atherosclerosis by reducing inflammatory responses partly through the NRF2 pathway in macrophages and endothelial cells[36], in which proved the role of ceramide metabolism controlled by *SMPD3* gene in the whole body in atherosclerosis[37]. However, deleting the SMPD3 in fibroblasts induced hyaluronan and cholesterol accumulation, which increased the pro-atherogenic risk[38]. Therefore, the role of adipocyte-specific SMPD3 in atherosclerosis is still unclear.

In this study, we found that activation of adipocyte HIF-1α upregulated SMPD3-mediated ceramide production, and then aggravated atherosclerosis by suppressing cholesterol elimination and enhancing local and circulating inflammation levels. Moreover, *Smpd3* was identified as a novel HIF-1α target gene. Pharmacological studies showed that inhibition of adipocyte HIF-1α by PX-478, a HIF-1α-specific inhibitor that functions at multiple levels through inhibition of both HIF-1α transcription and translation, had therapeutic effects on atherosclerosis in mice. Taken together, our study reveals a pivotal role of SMPD3 in the adipocyte−HIF-1α-induced atherosclerotic axis in a ceramide-dependent manner.

2. Materials and methods

2.1. Mice and experimental design

Adipocyte-specific HIF-1α knockout (*Hif1a*$^{\Delta Adipo}$) mice and adipocyte-specific HIF-1α transgenic (Ad*Hif1a*$^{LSL/LSL}$) mice were generated using the Cre-loxP system, as previously described[25,39,40]. *ApoE*$^{-/-}$ mice were obtained from the Animal Center of Peking University (Beijing, China). All the mice had a

C57BL/6J background. We mated *Hif1a*$^{fl/fl}$ and *Hif1a*$^{\Delta Adipo}$ mice with *ApoE*$^{-/-}$ mice to produce *Hif1a*$^{fl/fl}$ *ApoE*$^{-/-}$ and *Hif1a*$^{\Delta Adipo}$ *ApoE*$^{-/-}$ mice, respectively. Eight-week-old male mice were used and acclimatized to new environment for 1 week before the experiments. Atherosclerosis lesion was induced by treating a Western diet (WD; 42% fat, 0.2% total cholesterol, TD.88137, Harlan Teklad) for 8 weeks. Mice were housed in an SPF environment with a 12-h light and 12-h dark cycle. All animal procedures were performed under protocols approved by the Animal Care and Use Committee of Peking University, and approval was obtained from the Animal Research Ethics Committees of Peking University. In lentivirus-SMPD3 injection experiment, LV-SMPD3 (*Smpd3* cDNA was cloned into the lentivirus vector pLent-EF1a-FH-CMV-GFP-P2A-Puro) and LV-GFP (lentivirus vector pLent-EF1a-FH-CMV-GFP-P2A-Puro) were obtained from Hanheng (Shanghai, China). Eight-week-old *Hif1a*$^{\Delta Adipo}$ *ApoE*$^{-/-}$ mice were administered recombinant lentivirus or the corresponding vector (1×10^7 infection units per mouse) in the epididymal fat pad. The detailed operation method was previously described[41]. In the ceramide-treatment experiment, C16:0 ceramide (d18:1/16:0 ceramide; Avanti Polar Lipids, USA; #860516) was suspended in saline with 0.5% sodium carboxymethyl cellulose (NaCMC) and 5% Tween 80. Eight-week-old *Hif1a*$^{\Delta Adipo}$ *ApoE*$^{-/-}$ mice were intraperitoneally injected with vehicle or C16:0 ceramide (10 mg/kg) every other day with a WD for 6 weeks. In the PX-478-treatment experiment, PX-478 (5 mg/kg; MedChemExpress, China; #HY-10231) was dissolved in saline, and then, 8-week-old *ApoE*$^{-/-}$ mice were injected intraperitoneally with vehicle or PX-478 every other day for 8 weeks, respectively.

2.2. Cell culture

The 3T3-L1 cell line and HEK293T cell line were purchased from the Cell Resource Center of China (Beijing, China). The 3T3-L1 and HEK293T cells were cultured in Dulbecco's modified Eagle's medium−high glucose plus 10% fetal bovine serum in a 5% CO_2 atmosphere at 37 °C. For cells differentiation, 3T3-L1 cells were treated after reaching a confluence of 70%, and then covered cells were treated with insulin (5 μg/mL; Sigmae−Aldrich; #91077C), IMX (500 μmol/L; Abcam; #ab120840) and dexamethasone (0.1 μmol/L; Abcam; #ab120743) for 2 days. The medium was changed every other day.

2.3. Quantitative analysis of atherosclerotic lesion areas

To analyze atherosclerotic lesions, the entire *en face* aorta was visualized after staining with oil red O (Sigma−Aldrich). Pictures of aortas were captured by a digital camera that outfits a Canon EOS 650D lens (Canon) and then analyzed using ImageJ software. For histological analysis of atherosclerotic lesions in the aortic root, hearts were embedded in OCT compound. After solidification, the hearts were cut into serial 7-μm-thick sections using a Microm cryostat (for frozen blocks), stained with oil red O and counterstained with hematoxylin. Pictures were captured by an inverted microscope (Leica Microsystems Ltd., Milton Keynes, UK). The ratios of atherosclerotic lesions in the aortic roots were determined using ImageJ software.

2.4. Immunofluorescence analysis

Seven-μm-thick frozen cryosections of mouse aortic roots were used for detection of MAC-2 staining by immunofluorescence. Blocked with 5% BSA for 1 h, the sections were incubated with MAC-2 antibody (1:500; Cedarlane, Ontario, Canada; #CL8942AP) at 4 °C overnight. The next day, the sections were incubated with Alexa Fluor 488-conjugated rabbit anti-mouse IgG secondary antibody (red, 1:200; Invitrogen, CA, USA; #A-11006) at room temperature for 1 h in the dark, and the nuclei were stained with Hoechst 33342 to counterstain nuclei (blue, 1:1000; Invitrogen, CA, USA; #H3570) for 10 min. All immunofluorescence micrographs were acquired using confocal laser scanning microscopy (Leica Microsystems, Wetzlar, Germany) and analyzed by ImageJ software.

2.5. Immunological and biochemical assays

Plasma inflammatory cytokines were quantified using a cytometric bead array inflammation kit (BD Biosciences, CA, USA) and analyzed by a BD FACSCalibur (BD Biosciences, CA, USA). Total cholesterol and triglyceride levels were examined using commercial kits (BioSino Bio-Technology and Science, Beijing, China) according to the manuscript. For FPLC analysis, pooled plasma samples were injected into the machine with a Superose S-6 10/300 GL column (GE Healthcare, Sweden), and all the sequential fractions were collected, then each fraction of cholesterol concentrations was measured as described above.

2.6. RNA isolation and quantitative real-time PCR

Tissues and cells were suspended in TRIzol Reagent (Invitrogen, CA, USA), and total RNA was extracted according to the manufacturer's instructions. Reverse transcription was performed using a 5× All-In-One RT MasterMix kit (Abm, China). Real-time PCR was performed using a TransStart SuperMix (with Dye) kit (TransGen Biotech, China). All the primer sequences are shown in Supporting Information Table S1. All PCR samples were quantitated by the comparative CT method to obtain relative quantitation that was normalized to 18S.

2.7. Protein extraction and Western blotting

The proteins of tissues and cells were obtained using RIPA buffer (Beyotime Biotechnology, China), which added with 1% protease and phosphatase inhibitors as well as PMSF according to the standard manufacturer's instructions. Protein samples were quantified with BCA reagent (Pierce, USA), then separating total proteins by SDS-PAGE and electrophoretically transferred onto nitrocellulose membrane (NC). Chemiluminescence was used and then performed by using the LI-COR Odyssey Fc imager (LI-COR Biosciences, Lincoln, NE, USA). All analyses of proteins expression were performed using EIF5 as the internal control. Mouse monoclonal antibody against SMPD3 (Santa Cruz Biotechnology, Texas, USA; #sc-166637), mouse monoclonal antibody against HIF-1α (Novus, CO, USA; #NB100-105), rabbit polyclonal antibody against EIF5 (Santa Cruz Biotechnology, Texas, USA; #sc-282).

2.8. Luciferase reporter gene assays

The pGL3-basic luciferase reporter vector (Promega, WI, USA) was used, and the mouse *Smpd3* promoter was amplified and then cloned into the KpnI and XhoI sites of the vector. HEK293T cells were transfected with *Smpd3* reporter vectors, phRL-TK *Renilla* luciferase control vector (Promega, WI, USA) and HIF-1αTM (constitutively active HIF-1α triple mutants) expression plasmid

or the corresponding empty backbone vector (pcDNA3). Transfections were carried out using Lipofectamine 3000 (Invitrogen, CA, USA) according to the manufacturer's instructions. A dual-luciferase assay system (Promega, WI, USA) was used for luciferase assays after 24 h. The *Firefly*/*Renilla* luciferase ratio was quantified as the fold change relative to the control group.

2.9. Chromatin immunoprecipitation

As previously[42], 200 mmol/L cobalt (II) chloride hexahydrate was used to incubate differentiated 3T3-L1 adipocytes for 12 h. Remove the growth medium from 10 cm dishes and add 5 mL of cross-linking solution (4% formaldehyde) to each of the dishes. Place the dishes on a rotary shaker for 10 min at room temperature, and then stop the cross-linking reaction by adding glycine to a final concentration of 125 mmol/L for 5 min. Gently mix by rotating the reaction mixture for 10 min at room temperature. After washing with buffers, scrape the cells and collect them with SDS ChIP lysis buffer. Using an M220 (Covaris, MA, USA) connected to a cooling system (4 °C), sonicate the samples under high-power mode for ten cycles (30 s on/60 s off). Keep the samples on ice. Segregate the fragmented chromatin by centrifugation at 10,000×*g* for 5 min at 4 °C, and then dilute the supernatants in ChIP dilution buffer [1% Triton X-100, 2 mmol/L EDTA, 20 mmol/L Tris-HCl (pH 8.1), 150 mmol/L NaCl plus 10 mmol/L NAM and protease inhibitors]. Chromatin sections were rotated at 4 °C with magnetic beads (Dynabeads Protein A or G, Invitrogen) prebound with 2 μg of antibody. Then, the ChIP reactions were washed in the following buffers: TSE I, TSE II, buffer III and Tris·EDTA buffer. Incubate all washing reactions in the rotating thermomixer for 10 min at 4 °C. The sample was incubated under rotation overnight at 37 °C and then for another 2 h at 70 °C. DNA was purified by a PCR purification kit (Qiagen, Hilden, Germany) and quantitated by quantitative PCR (qPCR). The primer sequences are shown in Table S1.

2.10. Metabolomics analysis

Lipidomic experiments were performed according to a procedure described previously[41]. Briefly, for adipose tissue lipidomic analysis, approximately 20 mg of adipose tissue was homogenized in 200 μL of H_2O and then extracted with 1000 μL of precooled chloroform:methanol (2:1) solution containing LM6002 (Avanti Polar Lipids, Alabaster, AL, USA) as an internal standard. After centrifuged at 18,000×*g* for 5 min, the lower organic phase was collected to evaporate. For plasma lipidomic analysis, 200 μL of precooled chloroform:methanol (2:1) solution with LM6002 (Avanti Polar Lipids) was mixed with 50 μL of serum. Samples were centrifuged at 18,000×*g* for 5 min, and the lower organic phase was collected to evaporate. Then, the organic residue was re-dissolved in isopropanol:acetonitrile (1:1) solution for qualification. Eksigent LC100 coupled with an AB SCIEX Triple TOF 5600 system were used to analyze the samples. Peak extraction and integration were analyzed by Xcalibur 2.2 SP1.48 software (Thermo Fisher Scientific, Waltham, MA, USA).

2.11. Statistical analysis

Statistical analyses were performed with GraphPad Prism version 8.0 (GraphPad Software, San Diego, CA, USA). Experimental data are expressed as the mean ± standard error of mean (SEM). The Shapiro−Wilk normality test was used to determine the normal distribution of samples. Comparisons between two groups were performed by two-tailed unpaired Student's *t*-test (normal distribution) or Mann−Whitney U test (non-normal distribution). Comparisons across multiple groups were assessed with one-way ANOVA (normal distribution) or Kruskal−Wallis test (non-normal distribution), followed by Tukey's or Dunnett's T3 *post hoc* correction, as indicated in each figure legend.

3. Results

3.1. Adipocyte-specific HIF-1α disruption alleviates atherosclerosis

To determine the role of adipocyte HIF-1α in WD-induced atherosclerosis, we generated adipocyte-specific HIF-1α and APOE double knockout ($Hif1a^{\Delta Adipo}$ $ApoE^{-/-}$) mice and housed them with a WD for 8 weeks. In this model, $Hif1a^{\Delta Adipo}$ $ApoE^{-/-}$ mice show similar body weight compared to $Hif1a^{fl/fl}$ $ApoE^{-/-}$ mice (Supporting Information Fig. S1A). Adipose HIF-1α deficiency significantly reduced atherosclerotic lesions area, as indicated by oil red O staining of heart outflow tract (Fig. 1A and Fig. S1B). In keeping with these data, $Hif1a^{\Delta Adipo}$ $ApoE^{-/-}$ mice showed decreased levels of plasma total cholesterol and triglyceride compared to those in control mice (Fig. 1B and C). Since high level of LDL-C is a clear risk factor, which positively correlated with the occurrence of atherosclerosis, we carried out fast protein liquid chromatography (FPLC) to examine cholesterol levels in different plasma lipoprotein fractions. As expected, the plasma levels of very low-density lipoprotein (VLDL) cholesterol and LDL cholesterol were both lower in the $Hif1a^{\Delta Adipo}$ $ApoE^{-/-}$ mice than those in the $Hif1a^{fl/fl}$ $ApoE^{-/-}$ mice (Fig. 1D).

As abundant evidence proved, the interaction of LDL with macrophages in atherosclerotic plaques leads to increased inflammation[43]. We found the mRNA levels of the proinflammatory genes *Tnfa*, *Mcp1*, *Il1b*, and *Ccl5* were lower in the aortas of the $Hif1a^{\Delta Adipo}$ $ApoE^{-/-}$ mice than the $Hif1a^{fl/fl}$ $ApoE^{-/-}$ mice (Fig. 1E). Consistently, the circulating inflammatory cytokines MCP-1, TNF-α, and IL-6 were much lower in the $Hif1a^{\Delta Adipo}$ $ApoE^{-/-}$ mice than in control mice (Fig. 1F−H). Infiltration of macrophages in atherosclerotic plaques reflects severe inflammation and atherosclerotic plaque damage. MAC-2 expression of the aortic root sections detected by immunofluorescence demonstrated reduced macrophage contents in the $Hif1a^{\Delta Adipo}$ $ApoE^{-/-}$ mice compared to those of control mice (Fig. 1I).

3.2. Loss of adipocyte HIF-1α reduces proinflammatory ceramide levels

The harmful effects of adipocyte HIF-1α on atherosclerosis led us to investigate which key factor may alter the development of atherosclerosis. We then determined the pro-inflammatory lipid profiles. Partial least squares discriminant analysis (PLS-DA) modeling of lipid metabolites in epididymal white adipose tissue (eWAT) was different between the $Hif1a^{\Delta Adipo}$ $ApoE^{-/-}$ and $Hif1a^{fl/fl}$ $ApoE^{-/-}$ mice after fed a WD for 8 weeks (Fig. 2A). The variable importance for the projection (VIP) score analysis showed that the primary metabolites leading to clustering were ceramides and sphingolipids (Fig. 2B). We further quantified the concentrations of sphingolipids in the adipose tissue and plasma of

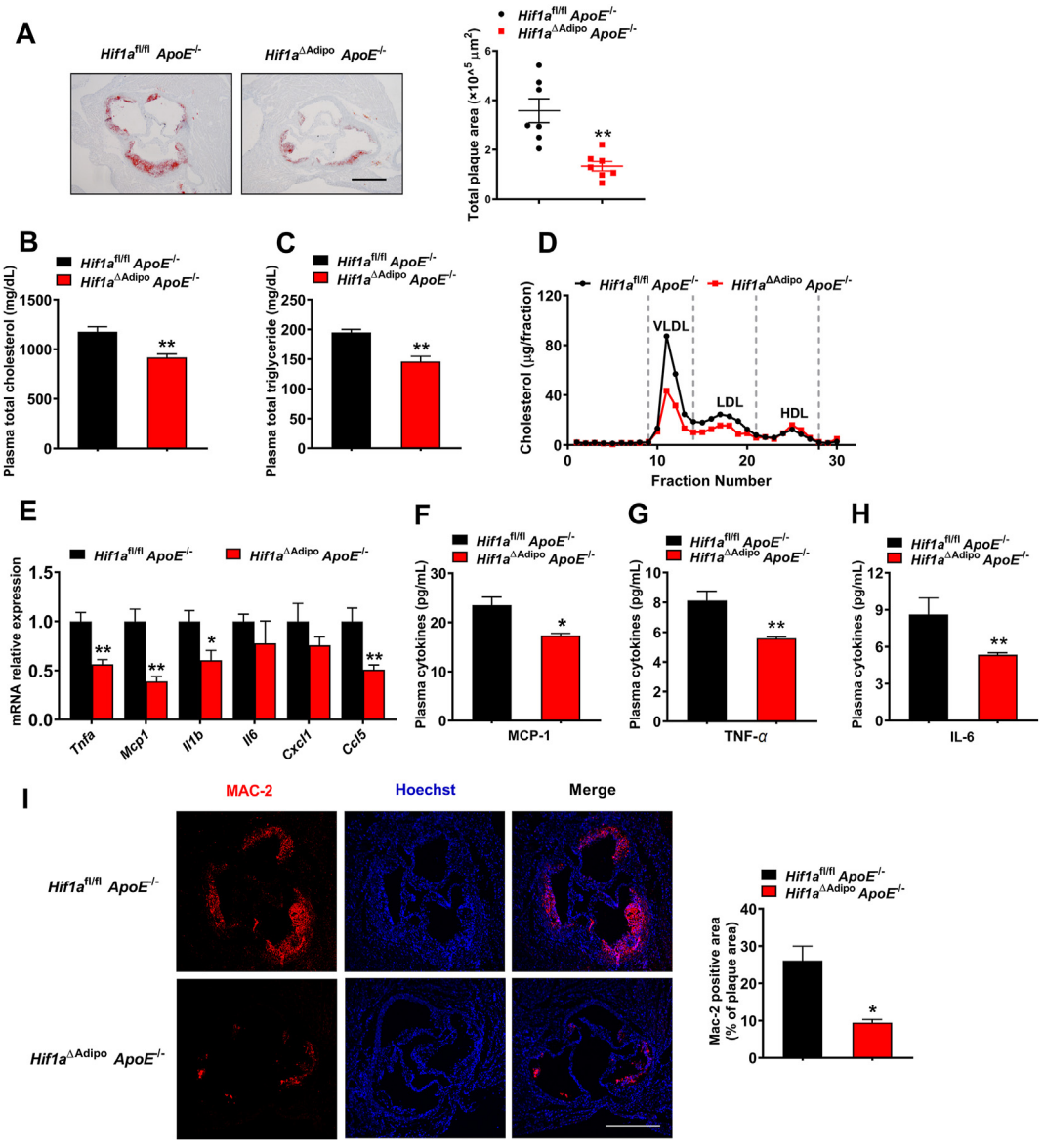

Figure 1 HIF-1α deficiency in adipocytes alleviates WD-induced atherosclerosis. Eight-week-old *Hif1a*$^{fl/fl}$ *ApoE*$^{-/-}$ and *Hif1a*$^{\Delta Adipo}$ *ApoE*$^{-/-}$ mice were fed a WD for 8 weeks. (A) Representative oil red O staining of cross-sections of aortic roots ($n = 7$ per group). Scale bar, 500 μm. (B, C) The levels of plasma total cholesterol (B) and triglyceride (C) in mice ($n = 6$ per group). (D) FPLC analysis of plasma cholesterol levels ($n = 3$ per group). (E) QPCR analysis of the *Tnfa*, *Mcp1*, *Il1b*, *Il6*, *Cxcl1*, and *Ccl5* mRNA levels in aortas ($n = 6$ per group). (F−H) The levels of the plasma cytokines MCP-1 (F), TNF-α (G), and IL-6 (H) in mice ($n = 6$ per group). (I) Immunofluorescence staining of atherosclerotic lesions with MAC-2 antibody and calculated MAC-2 positive areas in the plaques ($n = 3$ per group). Scale bar, 500 μm. All data are presented as the mean ± SEM. Two-tailed Student's *t*-test (A−C, E−I): $^*P < 0.05$, $^{**}P < 0.01$ compared to the *Hif1a*$^{fl/fl}$ *ApoE*$^{-/-}$ group. See also Fig. S1.

the *Hif1a*$^{\Delta Adipo}$ *ApoE*$^{-/-}$ and *Hif1a*$^{fl/fl}$ *ApoE*$^{-/-}$ mice by targeted lipidomics. The total and different species of ceramides and dihydroceramides were lower in the eWAT (Fig. 2C and D) and plasma (Fig. 2E and F) of the *Hif1a*$^{\Delta Adipo}$ *ApoE*$^{-/-}$ mice than those of the *Hif1a*$^{fl/fl}$ *ApoE*$^{-/-}$ mice. While levels of several sphingolipid metabolites such as SM16:0 and SM24:0 were higher in the eWAT (Supporting Information Fig. S2A) of the *Hif1a*$^{\Delta Adipo}$ *ApoE*$^{-/-}$ mice than the *Hif1a*$^{fl/fl}$ *ApoE*$^{-/-}$ mice, there was no difference in plasma (Fig. S2B). These findings indicate that defective lipid metabolism in atherosclerosis and adipocyte HIF-1α deficiency contributes to the protective response through decreasing proinflammatory ceramides level.

3.3. *Adipocyte HIF-1α modulates ceramide generation by regulating the expression of SMPD3*

To further elucidate the function of adipocyte HIF-1α in ceramide disorder, we measured the relative expression of genes involved in ceramide metabolism. In adipocyte specific HIF-1α overexpression (Ad*Hif1a*$^{LSL/LSL}$) mice, we observed significantly elevated mRNA levels of *Smpd3*, which regulates ceramide synthesis, in the eWAT of the Ad*Hif1a*$^{LSL/LSL}$ mice compared to vehicle (*Hif1a*$^{+/+}$) mice, while unaltered expression of ceramide catabolism genes, such as Acers (Fig. 3A). In addition, we also found lower *Cers6* and *Smpd3* expression in the *Hif1a*$^{\Delta Adipo}$ *ApoE*$^{-/-}$ mice than in the littermate

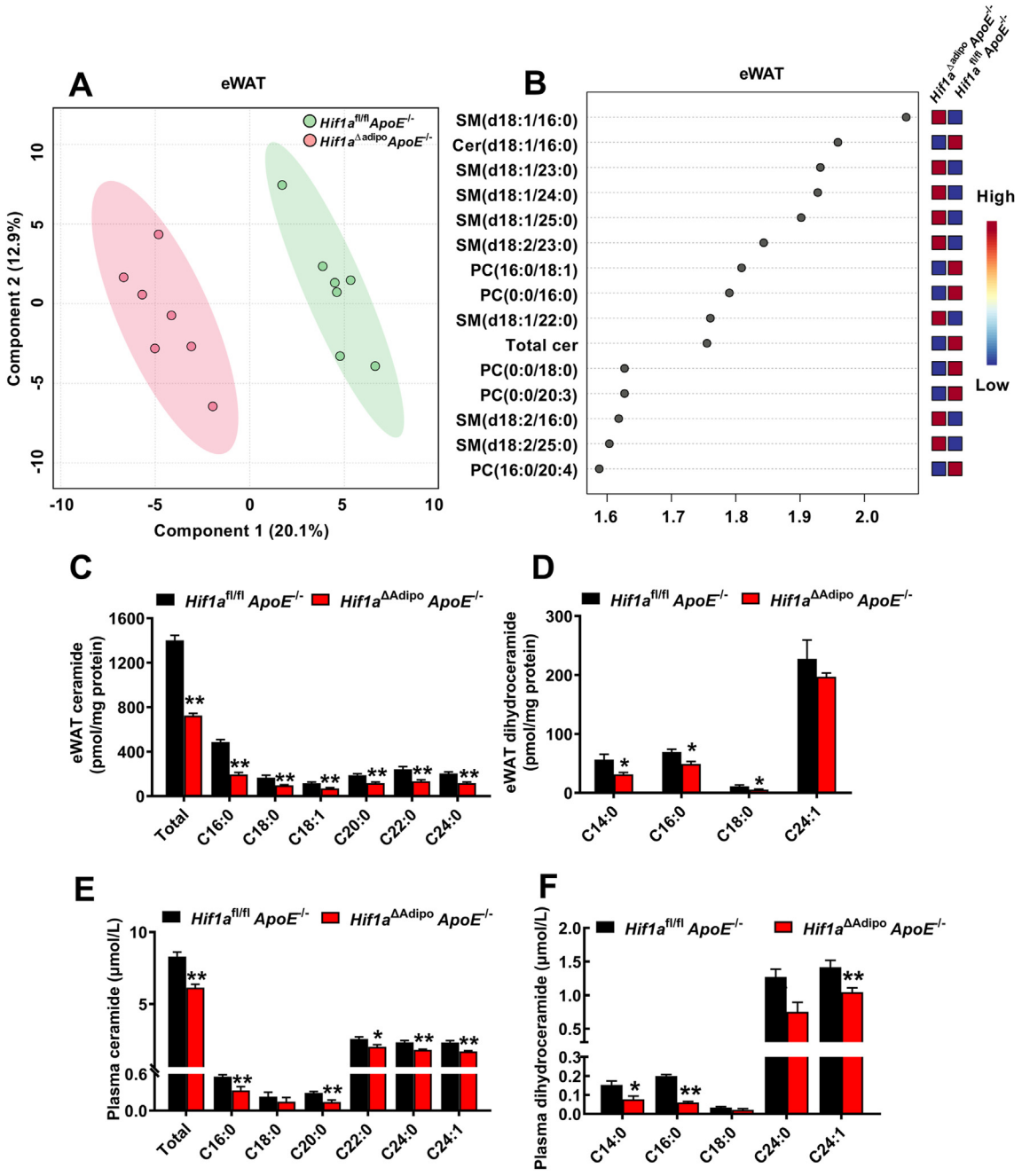

Figure 2 Adipocyte-specific HIF-1α ablation decreases ceramide generation. Eight-week-old *Hif1a*$^{fl/fl}$ *ApoE*$^{-/-}$ and *Hif1a*$^{\Delta Adipo}$ *ApoE*$^{-/-}$ mice were fed a WD for 8 weeks. (A) PLS-DA analysis of lipid metabolites in eWAT between the *Hif1a*$^{fl/fl}$ *ApoE*$^{-/-}$ (green circle) and *Hif1a*$^{\Delta Adipo}$ *ApoE*$^{-/-}$ (red circle) mice ($n = 7$ per group). (B) VIP score plot showing the top 15 lipid metabolites in eWAT. Normalized expression level of each metabolite in the *Hif1a*$^{\Delta Adipo}$ *ApoE*$^{-/-}$ mice compared to the *Hif1a*$^{fl/fl}$ *ApoE*$^{-/-}$ mice ($n = 7$ per group). (C, D) Quantitation of ceramide (C) and dihydroceramide (D) concentrations in eWAT ($n = 7$ per group). (E, F) Quantitation of ceramide (E) and dihydroceramide (F) concentrations in plasma ($n = 7$ per group). All data are presented as the mean ± SEM. Mann−Whitney U test (C, D) and two-tailed Student's *t*-test (E, F): $^*P < 0.05$, $^{**}P < 0.01$ compared to the *Hif1a*$^{fl/fl}$ *ApoE*$^{-/-}$ group. See also Fig. S2.

control mice (Fig. 3C). Similarly, the protein level of SMPD3 in eWAT was consistently changed between the compared groups (Fig. 3B and D). Based on these results, *Smpd3* may be a potential target gene of adipocyte HIF-1α. To confirm this hypothesis, we analyzed the *Smpd3* promoter and identified putative HIF-response elements (HREs) in the promoter region of *Smpd3* (Fig. 3E). Thus, we performed chromatin immunoprecipitation (ChIP) assays to validate whether HIF-1α bound to this site, and under $CoCl_2$ stimulated condition, mimicking a hypoxia environment, enhanced the binding of HIF-1α to the HRE in 3T3-L1 cells (Fig. 3F). Similarly, luciferase reporter assays further revealed increased transcriptional activity of the *Smpd3* promoter after overexpression of a constitutively active HIF-1α triple mutant (HIF-1αTM) expression plasmid in HEK293T cells, while the increased reporter

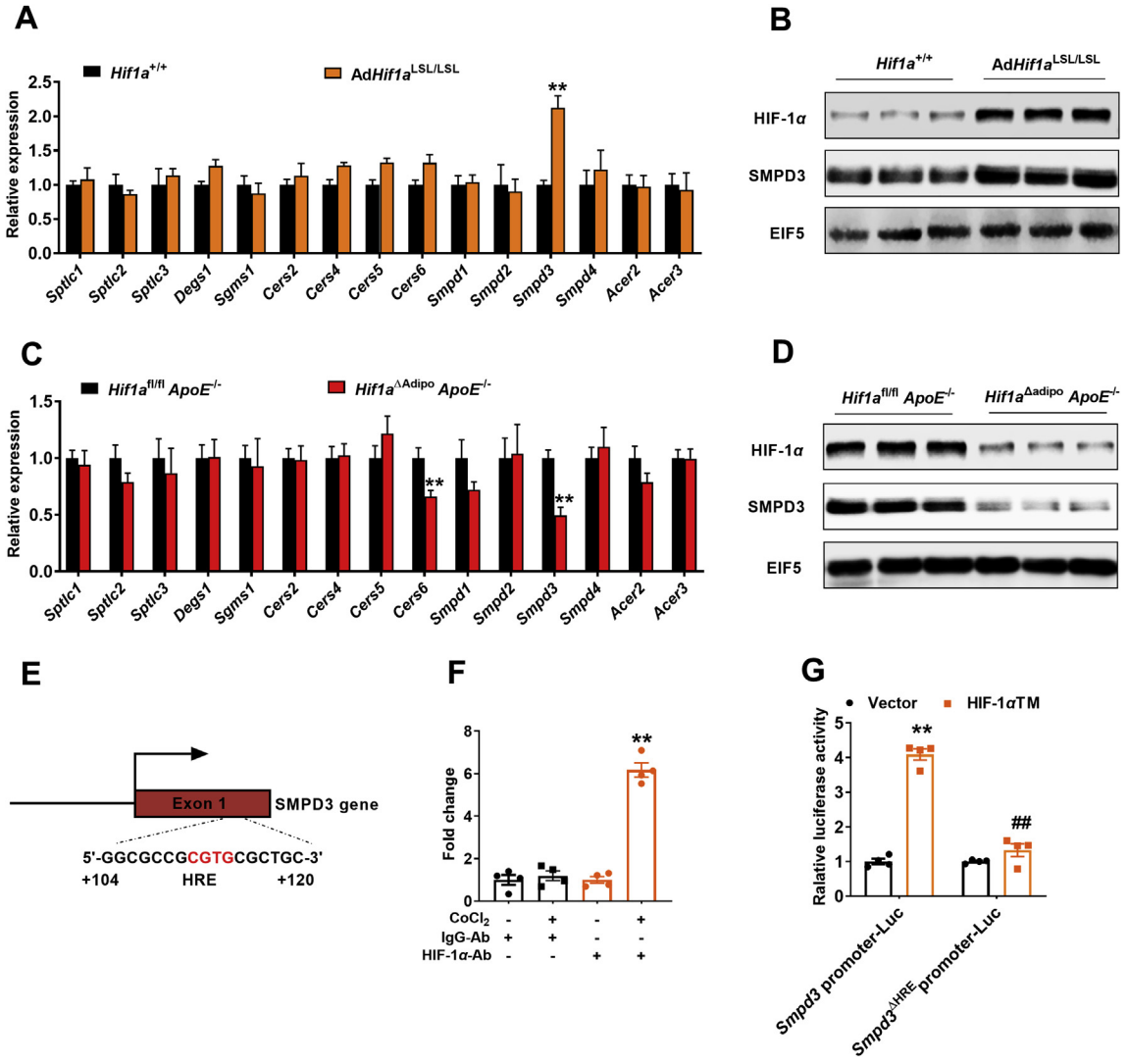

Figure 3 The ceramide-generation-related gene *Smpd3* is a novel target gene of adipocyte HIF-1α. (A) The mRNA levels of genes related to ceramide metabolism, including synthesis, transportation and elimination in the eWAT of the Ad*Hif1a*$^{LSL/LSL}$ and *Hif1a*$^{+/+}$ mice ($n = 6$ per group). Two-tailed Student's *t*-test: $^{**}P < 0.01$ compared to the *Hif1a*$^{+/+}$ mice. (B) The protein levels of HIF-1α and SMPD3 in the eWAT of the Ad*Hif1a*$^{LSL/LSL}$ and *Hif1a*$^{+/+}$ mice ($n = 3$ per group). (C) The mRNA levels of genes related to ceramide metabolism, including synthesis, transportation and elimination in the eWAT of the *Hif1a*$^{fl/fl}$ *ApoE*$^{-/-}$ and *Hif1a*$^{\Delta Adipo}$ *ApoE*$^{-/-}$ mice fed a WD for 8 weeks ($n = 6$ per group). Two-tailed Student's *t*-test: $^{**}P < 0.01$ compared to the *Hif1a*$^{fl/fl}$ *ApoE*$^{-/-}$ mice. (D) The protein levels of HIF-1α and SMPD3 in the eWAT of the *Hif1a*$^{fl/fl}$ *ApoE*$^{-/-}$ and *Hif1a*$^{\Delta Adipo}$ *ApoE*$^{-/-}$ mice mice fed a WD for 8 weeks ($n = 3$ per group). (E) Schematic diagram of the mouse *Smpd3* promoter illustrating the predicted HRE in the regulatory region. The upstream regions are numbered in relation to the transcription initiation site, which is designated +1. (F) ChIP assays of 3T3-L1 adipocytes treated with $CoCl_2$ (200 μmol/L) for 12 h ($n = 4$ per group). One-way ANOVA with Tukey's *post hoc* test: $^{**}P < 0.01$ compared to the IgG-Ab group. (G) Luciferase reporter gene assay of *Smpd3* promoter activity ($n = 4$ per group). One-way ANOVA with Dunnett's T3 *post hoc* test: $^{**}P < 0.01$ compared to the *Smpd3* promoter plasmid with vector group; $^{\#\#}P < 0.01$ compared to the *Smpd3* promoter plasmid with HIF-1α TM group.

gene activity was eliminated when the HRE was mutated (Fig. 3G). These data indicate that HIF-1α directly regulated *Smpd3* transcription expression *via* binding to the HRE of the *Smpd3* promoter.

3.4. *Overexpression of SMPD3 in adipose tissue reverses the alleviation of atherosclerosis induced by adipocyte HIF-1α deficiency*

Next, we explored the role of SMPD3 on HIF-1α-induced ceramide production and secretion *in vivo*. Specific lentivirus carrying the mouse *Smpd3* cDNA sequence was designed and injected directly into the eWAT pats of the *Hif1a*$^{\Delta Adipo}$ *ApoE*$^{-/-}$ mice to rescue SMPD3 expression (Fig. 4A). QPCR and Western blot analysis confirmed that the *Hif1a*$^{\Delta Adipo}$ *ApoE*$^{-/-}$ + SMPD3 mice showed an increase in SMPD3 in the eWAT compared to the *Hif1a*$^{\Delta Adipo}$ *ApoE*$^{-/-}$ + GFP mice (Supporting Information Fig. S3A and S3B). As expected, the decreased adipocyte ceramide production and ceramide levels in serum due to adipocyte HIF-1α knockout were increased to similar levels as those in the control mice after forced SMPD3 expression (Fig. 4B and C). Moreover, the reduction of lesion area in the *Hif1a*$^{\Delta Adipo}$ *ApoE*$^{-/-}$ mice was partially reversed by the overexpression of SMPD3 in both the

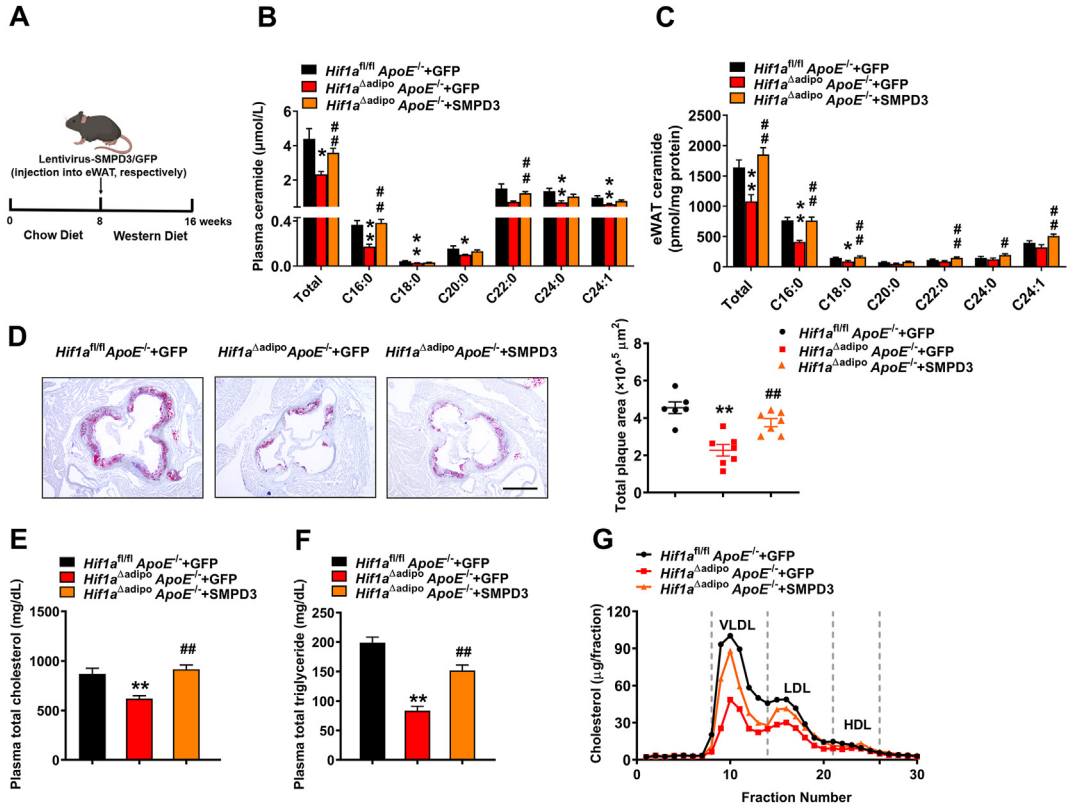

Figure 4 Overexpression of SMPD3 in adipose tissue aggravates the progression of atherosclerosis. Eight-week-old *Hif1a*$^{fl/fl}$ *ApoE*$^{-/-}$ and *Hif1a*$^{\Delta Adipo}$ *ApoE*$^{-/-}$ mice were injected with lentivirus carrying mouse *Smpd3* cDNA sequence or green fluorescent protein (GFP) and were fed a WD for 8 weeks. (A) Schematic diagram of the mouse model illustrating the concept of mouse injection with lentivirus-SMPD3/GFP. (B, C) Quantitation of ceramide concentrations in plasma (B) and eWAT (C), $n = 6$ per group. (D) Representative oil red O staining of cross-sections of aortic roots ($n = 6$–7 per group). Left, representative examples of cross-sections from the aortic root stained with oil red O. Scale bar, 500 μm. Right, quantification of aortic root lesion areas. (E, F) The levels of plasma total cholesterol (E) and triglyceride (F) in mice ($n = 6$–7 per group). (G) FPLC analysis of plasma cholesterol levels in mice. All data are presented as the mean ± SEM. one-way ANOVA with Tukey's *post hoc* test (B–F): $^{*}P < 0.05$, $^{**}P < 0.01$ compared to the *Hif1a*$^{fl/fl}$ *ApoE*$^{-/-}$ + GFP group; $^{\#}P < 0.05$, $^{\#\#}P < 0.01$ compared to the *Hif1a*$^{\Delta Adipo}$ *ApoE*$^{-/-}$ + GFP group. See also Fig. S3.

whole aortic and cross-sections of aortic roots (Fig. 4D and Fig. S3C), and the lower total cholesterol and triglyceride levels, especially VLDL and LDL cholesterol, in the plasma of the *Hif1a*$^{\Delta Adipo}$ *ApoE*$^{-/-}$ + GFP mice than the *Hif1a*$^{fl/fl}$ *ApoE*$^{-/-}$ + GFP mice were also aggravated due to rescued SMPD3 overexpression (Fig. 4E–G). Together, these results demonstrate that adipocyte HIF-1α promotes atherosclerosis progression *via Smpd3* expression regulation.

3.5. *Overexpression of SMPD3 in adipose tissue exacerbates the inflammation in atherosclerosis improved by adipocyte HIF-1α deficiency*

The latest studies and clinical evidence indicated that atherosclerosis is a chronic inflammatory disease[44]. We then determined the effect of overexpression of *Smpd3* in adipose tissue on inflammation. As assessed by biochemical analysis, detection of MCP-1, TNF-α, and IL-6 levels in plasma showed that the *Hif1a*$^{\Delta Adipo}$ *ApoE*$^{-/-}$ + SMPD3 mice reversed the anti-inflammatory effect of the *Hif1a*$^{\Delta Adipo}$ *ApoE*$^{-/-}$ + GFP mice (Fig. 5A–C). Consistently, upregulation of the macrophage marker MAC-2 was observed in the atherosclerotic lesions of *Hif1a*$^{\Delta Adipo}$ *ApoE*$^{-/-}$ + SMPD3 mice compared to the *Hif1a*$^{\Delta Adipo}$ *ApoE*$^{-/-}$ + GFP mice (Fig. 5D), suggesting adipocyte SMPD3 overexpression exacerbated inflammation level in atherosclerosis through ceramide generation.

3.6. *Ceramide aggravates WD-induced dyslipidemia*

In order to determine the mechanisms underlying of ceramide in diet-induced atherosclerosis, we quantified the effect of additional administration of C16:0 ceramide on the progression of atherosclerosis (Fig. 6A). We found several species of ceramide in the plasma and eWAT of the *Hif1a*$^{\Delta Adipo}$ *ApoE*$^{-/-}$ mice with C16:0 ceramide increased after injection (Fig. 6B and C), which reversed the decreased ceramide profiles in the *Hif1a*$^{\Delta Adipo}$ *ApoE*$^{-/-}$ mice. The levels of plasma total cholesterol and triglyceride, especially VLDL and LDL cholesterol, were higher in the *Hif1a*$^{\Delta Adipo}$ *ApoE*$^{-/-}$ mice treated with C16:0 ceramide than in the *Hif1a*$^{\Delta Adipo}$ *ApoE*$^{-/-}$ mice (Fig. 6D–F). As described previously, ceramide was found to reduce hepatic cholesterol elimination and aggravate dyslipidemia[41]. Then we further observed higher hepatic cholesterol and triglyceride levels in the *Hif1a*$^{\Delta Adipo}$ *ApoE*$^{-/-}$ mice treated with C16:0 ceramide than in the *Hif1a*$^{\Delta Adipo}$ *ApoE*$^{-/-}$ mice (Supporting Information Fig. S4A and S4B). Moreover, the mRNA expression of the *Cyp7a1* and *Abcg5* genes involved in cholesterol elimination was lower in the *Hif1a*$^{\Delta Adipo}$ *ApoE*$^{-/-}$ mice treated with C16:0 ceramide than in

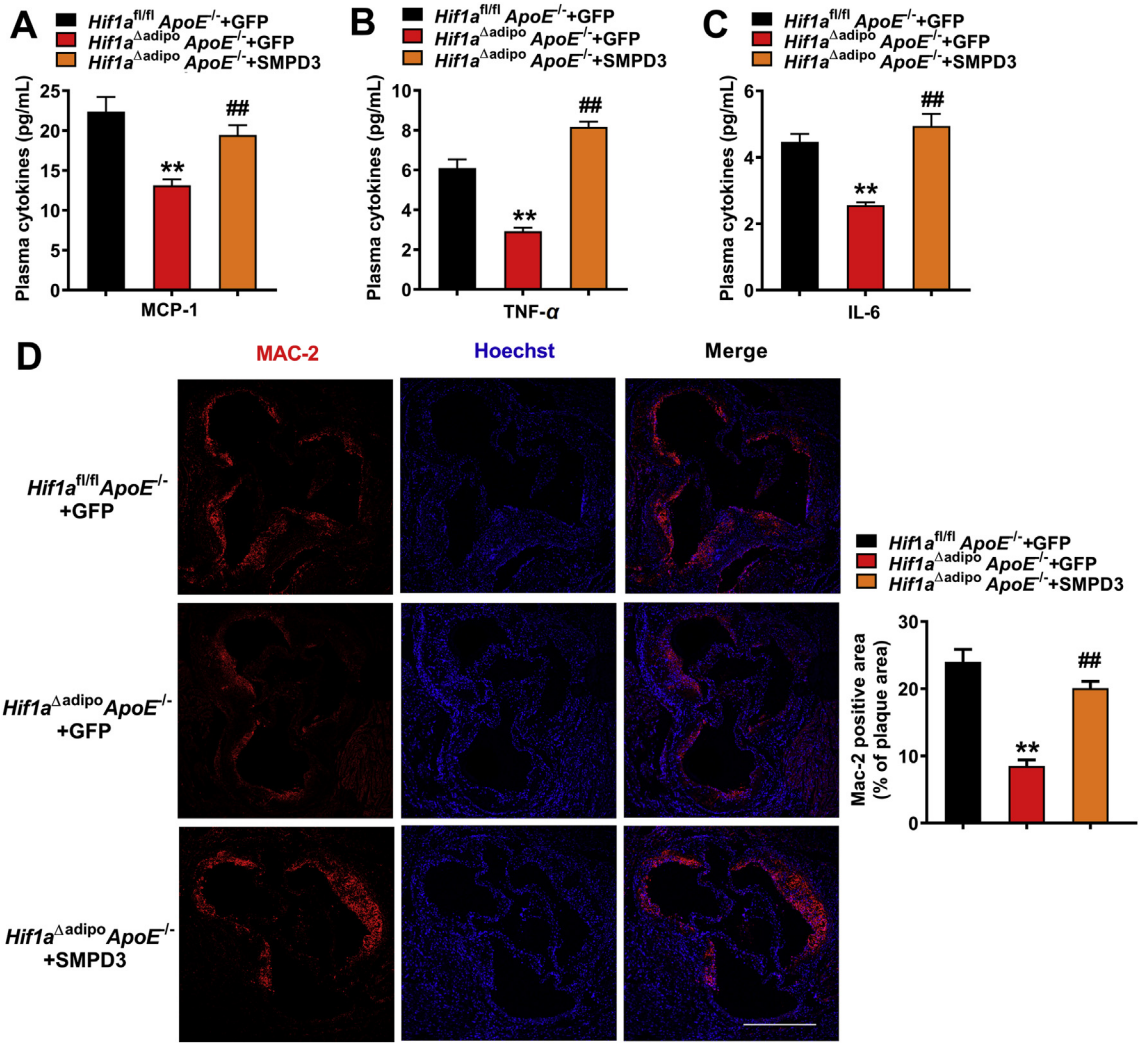

Figure 5 Lenti-SMPD3 aggravates inflammation. Eight-week-old *Hif1a*$^{fl/fl}$ *ApoE*$^{-/-}$ and *Hif1a*$^{\Delta Adipo}$ *ApoE*$^{-/-}$ mice were injected with lentivirus carrying mouse *Smpd3* cDNA sequence or GFP and were fed a WD for 8 weeks. (A−C) The levels of the plasma cytokines MCP-1 (A), TNF-α (B), and IL-6 (C) in mice ($n = 6$ per group). (D) Immunofluorescence staining of atherosclerotic lesions with MAC-2 antibody and calculated MAC-2 positive areas in the plaques ($n = 3$ per group). Scale bar, 500 μm. All data are presented as the mean ± SEM. One-way ANOVA with Tukey's *post hoc* test (A−D): $^{**}P < 0.01$ compared to the *Hif1a*$^{fl/fl}$ *ApoE*$^{-/-}$ + GFP group; $^{\#\#}P < 0.01$ compared to the *Hif1a*$^{\Delta Adipo}$ *ApoE*$^{-/-}$ + GFP group.

the *Hif1a*$^{\Delta Adipo}$ *ApoE*$^{-/-}$ mice (Fig. S4C). Consistently, oil red O staining exhibited increased atherosclerosis lesions, and proinflammatory cytokine levels and macrophage infiltration rate were also higher in the *Hif1a*$^{\Delta Adipo}$ *ApoE*$^{-/-}$ mice treated with C16:0 ceramide than those treated with vehicle (Fig. 6G, H, and Fig. S4D−S4F).

3.7. Administration of PX-478 reduces atherosclerosis in a HIF-1α-dependent manner

Because of the harmful role of adipocyte HIF-1α in atherosclerotic development, we explored the therapeutic effect of selective HIF-1α inhibitor PX-478, which inhibits HIF-1α protein levels in cancer models and improved diet-induced adipose tissue dysfunction[45], on atherosclerosis. PX-478 was intraperitoneally administered to *ApoE*$^{-/-}$ mice (Fig. 7A). The mRNA level of *Smpd3* and the protein levels of HIF-1α and SMPD3 were inhibited in the eWAT of the *ApoE*$^{-/-}$ mice after PX-478 administration compared to those of the vehicle group (Supporting Information Fig. S5A and S5B). Analysis of whole aortas and sections demonstrated that the PX-478-treated *ApoE*$^{-/-}$ mice had smaller lesions than the vehicle-treated mice (Fig. 7B and Fig. S5C). Furthermore, PX-478 treatment attenuated the ceramide levels in the plasma and eWAT of the *ApoE*$^{-/-}$ mice (Fig. 7C and D). The levels of plasma total cholesterol and triglyceride were lower after PX-478 treatment in the *ApoE*$^{-/-}$ mice than in the vehicle-treated mice (Fig. 7E−G). After staining for macrophage infiltration of the aortic root, we also found a lower level of the macrophage marker MAC-2 in the *ApoE*$^{-/-}$ mice after PX-478 administration than in the control mice (Fig. 7H). The plasma MCP-1, TNF-α, and IL-6 levels were also reduced in the *ApoE*$^{-/-}$ mice after PX-478 administration than the control mice (Fig. S5D−S5F). Hence, these results demonstrate the potential therapeutic function of PX-478 in atherosclerosis through inhibiting HIF-1α.

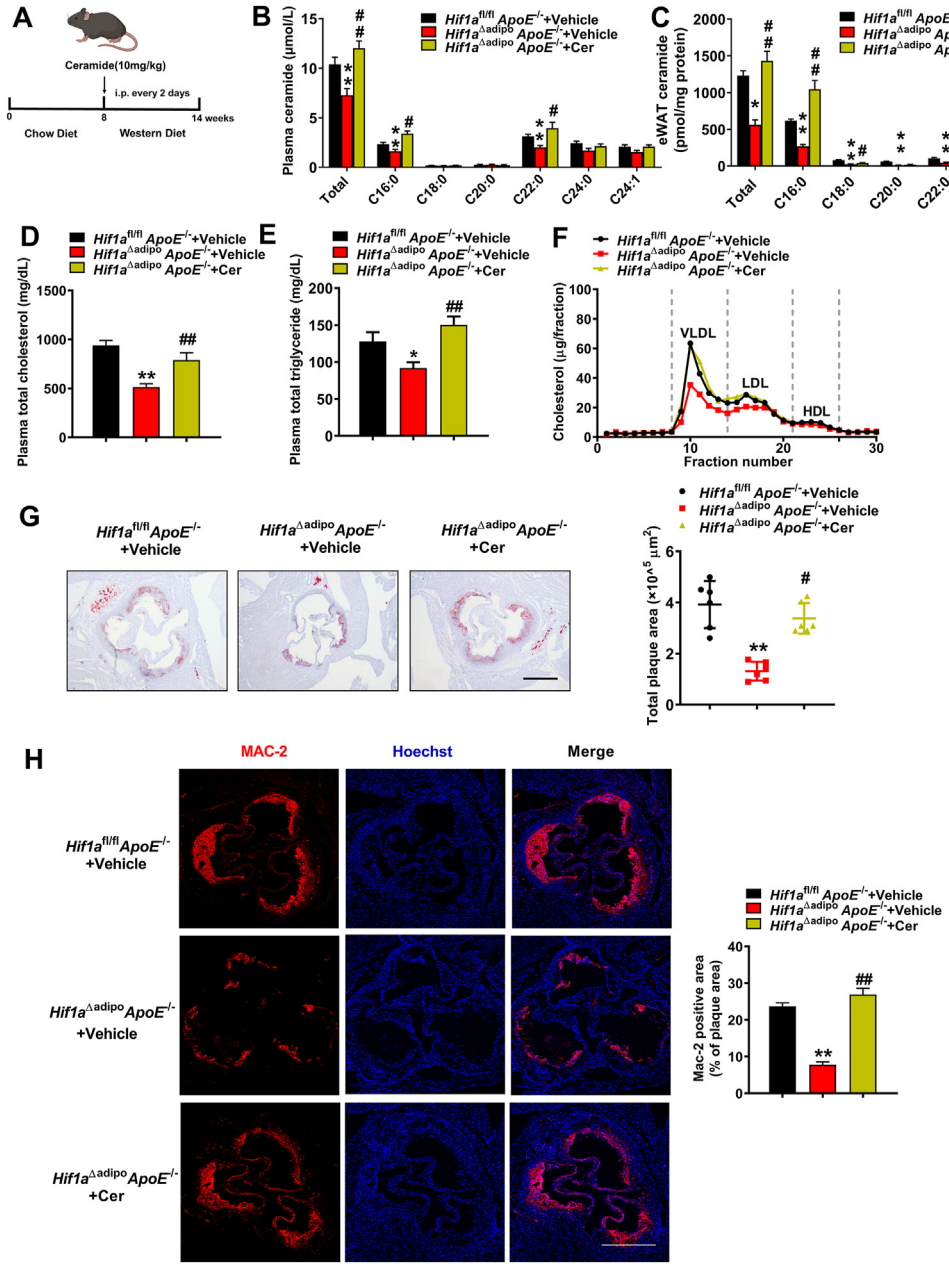

Figure 6 Administration of ceramide reverses the protective effects of adipose HIF-1α deficiency on atherosclerosis through increased inflammation and cholesterol. Eight-week-old *Hif1a*$^{fl/fl}$ *ApoE*$^{-/-}$ and *Hif1a*$^{\Delta Adipo}$ *ApoE*$^{-/-}$ mice were injected with ceramide C16:0 or vehicle and were fed a WD for 6 weeks. (A) Schematic diagram of the mouse model illustrating the concept of mouse injection with ceramide C16:0 or vehicle. (B, C) Quantitation of ceramide concentrations in plasma (B) and eWAT (C), $n = 6$ per group. (D, E) The levels of plasma total cholesterol (D) and triglyceride (E), $n = 6-7$ per group. (F) FPLC analysis of plasma cholesterol levels in mice. (G) Left, representative oil red O staining of cross-sections of aortic roots. Scale bar, 500 μm. Right, quantification of aortic root lesion areas. $n = 6-7$ per group. (H) Immunofluorescence staining of atherosclerotic lesions with MAC-2 antibody and calculated MAC-2 positive areas in the plaques ($n = 3$ per group). Scale bar, 500 μm. All data are presented as the mean ± SEM. One-way ANOVA with Tukey's *post hoc* test (B, D, E, H) and Kruskal–Wallis test (C and G): $^{*}P < 0.05$, $^{**}P < 0.01$ compared to the *Hif1a*$^{fl/fl}$ *ApoE*$^{-/-}$ + vehicle group; $^{\#}P < 0.05$, $^{\#\#}P < 0.01$ compared to the *Hif1a*$^{\Delta Adipo}$ *ApoE*$^{-/-}$ + vehicle group. See also Fig. S4.

4. Discussion

The main finding of this study is that adipocyte HIF-1α accelerated WD-induced atherosclerosis by increasing ceramide levels. Loss-of-function and gain-of-function studies showed that adipocyte HIF-1α directly regulates *Smpd3*, which encodes neutral SMase, an enzyme that generates the bioactive lipid ceramide. These findings indicate a central role for the adipocyte HIF-1α-ceramide signaling axis in the pathogenesis of atherosclerosis. Furthermore, we observed that PX-478 played a protective role in the progression of atherosclerosis through inhibition of adipocyte ceramide production.

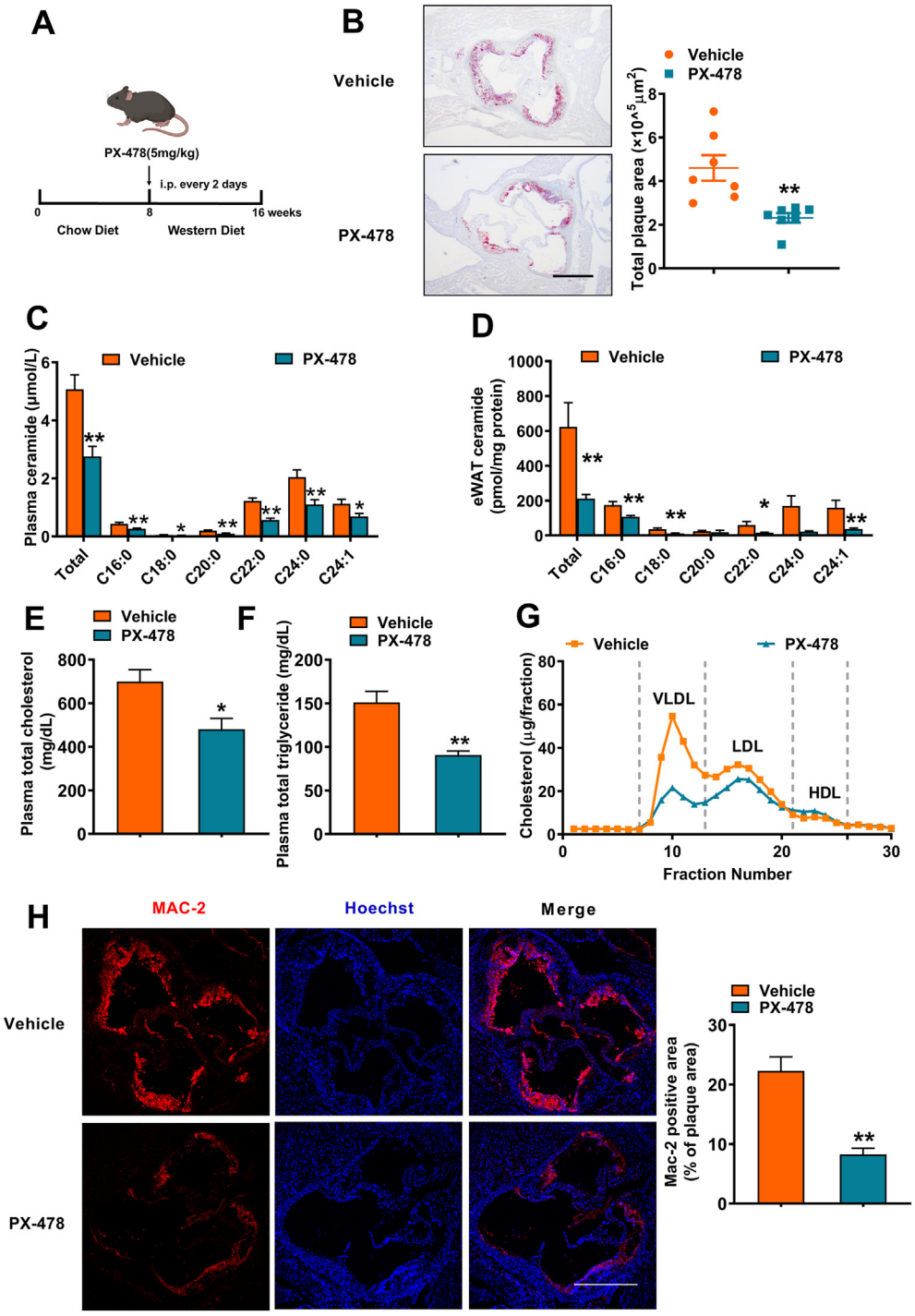

Figure 7 Inhibition of HIF-1α by PX-478 improves atherosclerosis through the SMPD3−ceramide axis. Eight-week-old *ApoE*$^{-/-}$ mice were administered with PX-478 (5 mg/kg) or vehicle every other day and fed a WD for 8 weeks. (A) Schematic diagram of the mouse model illustrating the concept of mouse injection with PX-478. (B) Left, representative oil red O staining of cross-sections of aortic roots. Scale bar, 500 μm. Right, quantification of aortic root lesion areas. $n = 7$ per group. (C, D) Quantitation of ceramide concentrations in plasma (C) and eWAT (D), $n = 6$ per group. (E, F) The levels of plasma total cholesterol (E) and triglyceride (F), $n = 7$ per group. (G) FPLC analysis of plasma cholesterol levels in mice. (H) Immunofluorescence staining of atherosclerotic lesions with MAC-2 antibody and calculated MAC-2 positive areas in the plaques ($n = 3$ per group). Scale bar, 500 μm. All data are presented as the mean ± SEM. Mann−Whitney U test (B, D), Two-tailed Student's *t*-test (C, E, F, H): $^*P < 0.05$, $^{**}P < 0.01$ compared to the vehicle group. See also Fig. S5.

An increased visceral white adipose tissue (WAT) mass enhances the risk of developing cardiovascular diseases[46]. Due to limited O_2 diffusion into hypertrophic adipocytes, cellular hypoxia is observed in adipose tissue. Recent reports have demonstrated that adipose tissue HIF-2α reduces atherosclerosis *via* promoting ceramide catabolism and thus increasing hepatic cholesterol elimination and thermogenesis[41]. Unlike adipocyte HIF-2α is significantly inhibited with treated western diet, HIF-1α in adipose

tissue is significantly activated, which indicates that adipose HIF-1α activation is associated with metabolic disorders. Furthermore, HIFs are themselves regulated in a non-equivalent manner, where HIF-2α is typically stabilized at higher relative O_2 concentrations compared with HIF-1α[17]. They also exert different regulation on divergent target genes in interaction with alternative transcription factors and coregulators[20].

HIF-1α deletion in macrophages specifically reduced atherosclerosis and necrotic core formation through limiting macrophage necroptosis and necrotic core formation in *ApoE*$^{-/-}$ mice[47]. In occurrence of atherosclerosis, except for the vascular lesion *in situ*, the crosstalk between multiple organs is of profound impact as well[48]. Although it has been reported that adipose HIF-1α activation is associated with metabolic disorders such as insulin resistance and inflammation in obesity[16,49], the impact of adipose HIF-1α in atherosclerosis progression still unclarified. Activated HIF-1α signaling may aggravate dyslipidemia, inflammation and associated metabolic dysfunction, which could be common key factors in the pathogenesis of atherosclerosis[17,21]. In the present study, we observed that activated adipocyte HIF-1α signaling aggravated atherosclerosis by upregulating plasma total cholesterol, especially VLDL cholesterol and LDL cholesterol levels (Fig. 1B−D). In addition to its role in modulating lipid metabolism, this pathway may promote atherosclerosis by increasing circulating cytokine levels and local inflammation. Based on these results, we investigated the molecular mediators linking HIF-1α signaling and atherosclerosis.

Lipidomic analysis of different lipid fractions demonstrated that epididymal adipose tissue and plasma-derived ceramides and dihydroceramides were key mediators in the progression of atherosclerosis in our studies. Sphingolipid metabolites, particularly ceramide, sphingosine-1-phosphate (S1P) and sphingomyelin, are important signal molecules to regulate several cellular processes in immunity and inflammatory disorders[50]. Unlike ceramide, S1P has potent but opposing regulatory roles in numerous cell types, whereas S1P promotes vasodilatation and is atheroprotective[51]. Meanwhile, human plasma SM levels are positively and independently related to coronary artery disease[52]. Genetic ablation of the *Sgms2* gene in mice with or without *Apoe* knockout reduced plasma-membrane levels of sphingomyelin, increased insulin sensitivity[53] and ameliorated features of atherosclerosis[54]. Ceramide has also been regarded as a primary lipid mediator of obesity and inflammation[55,56]. While the change of ceramides was the most significant among sphingolipid metabolites in our animal models. Then, we examined the pathways of ceramide metabolism regulated by *de novo* synthesis, sphingomyelin hydrolysis and salvage pathways in different models. In the present study, we found that the impact of HIF-1α on ceramide metabolism is associated with neutral SMase 2 (nSMase2), a strongly altered enzyme that generates the bioactive lipid ceramide through the hydrolysis of the membrane lipid sphingomyelin in different models. The previous literature has proved SMPD3 knocked out systemically could reduce atherosclerosis[36]. Meanwhile, Angel and his colleague found that hypoxia increased ceramide content in isolated rat pulmonary artery smooth muscle cells which was abrogated by inhibition of nSMase but not aSMase[57]. Ceramide and reactive oxygen species production were increased by hypoxia in pulmonary arteries[58]. Based on previous studies and our results, adipose-derived ceramide is most likely mediated by HIF-1α-SMPD3 induction.

Ceramide has been shown to stimulate TNF-α and IL-6 production in cultured macrophages through NF-κB activation[59]. Furthermore, inflammation can reversely exacerbate the ceramide synthesis[60]. Interestingly, IL-1β was first reported to induce nSMase activity in rat hepatocytes, and nSMase2-derived ceramide also shows bioactivity itself in response to TNF-α and IFN-γ[33]. In agreement with Tom group who reported that nSMase2 deficiency or inhibition could reduce atherosclerosis with a decrease in macrophage infiltration and lipid deposition[36]. We also found that administration of C16:0 ceramide increased plasma cytokines of MCP-1, TNF-α and IL-6, as well as MAC-2 expression in atherosclerotic lesions in *Hif1a*$^{\Delta Adipo}$ *ApoE*$^{-/-}$ mice, which reversed the improvement of atherosclerosis (Fig. 6H and Fig. S4D−S4F). We also observed that induced changes in ceramide species of eWAT and plasma in our animal models (Fig. 6B and C). In general, ceramides exacerbated atherosclerosis at least partially through raising inflammatory cytokine production in the circulation.

Previously, hepatic cholesterol was shown to be excreted directly and indirectly through bile; thus, activation of hepatic cholesterol elimination through biliary excretion can reduce plasma cholesterol levels[42,61]. Based on our study, a similar inhibitory effect of ceramide on hepatic cholesterol elimination *via* suppression of hepatic *Cyp7a1* and *Abcg5* was observed (Fig. S4C). As described previously, the ceramide catabolism enzyme ACER2 is inhibited in eWAT, which in turn leads to the accumulation of ceramide[42]. In our model, HIF-1α in adipose tissue is significantly accumulated, which activates the synthesis pathway of sphingomyelin to ceramide and increases the content of ceramide through activated SMPD3. We also confirmed the role of ceramide in causing atherosclerosis to promote inflammation and increase the content of cholesterol. All of these findings can be explained in part by ceramide-induced atherosclerosis *via* increased inflammation and impaired cholesterol metabolism. Based on these results, we postulate that the regulation of lipid metabolism and inflammation by ceramides could be one of the possible mechanisms of diet-induced atherosclerosis.

"Ceramide reduction therapies", such as inhibiting ceramide biosynthesis or catalyzing ceramide degradation in rodents, is a good strategy to ameliorate many metabolic disorders[28]. We demonstrated the ceramide-lowering effects of PX-478, a selective HIF-1α inhibitor. PX-478 inhibits HIF-1α at multiple levels through inhibition of both HIF-1α transcription and translation[23,62] and is approved for advanced solid tumors/lymphoma in Phase I. Although these effects have not been confirmed to be driven by inhibition of adipocyte-derived ceramide production, an alternative source of ceramide is SM hydrolysis by SMase, which is directly activated by HIF-1α, and the present data suggested that this pathway is likely affected by PX-478 inhibition of HIF-1α signaling. Previous studies showed PX-478 significantly reduced plasma and total cholesterol levels in mice administered a high-fat diet. Furthermore, PX-478-treated mice displayed decreased macrophage infiltration, and the local mRNA levels of IL-6 were significantly suppressed by PX-478 treatment, suggesting that this treatment reduces inflammation[23]. These results indicate that PX-478 could be an anti-atherosclerotic agent. We further demonstrated that plasma cholesterol and circulating pro-inflammatory cytokines reduced after PX-478 treatment, accompanied by reduced macrophage infiltration in the plaque. PX-478 suppressed atherosclerosis, which could mainly depend on HIF-1α-ceramide metabolic regulation.

Here, we clarify the deleterious role of adipocyte−HIF-1α in atherosclerosis. Using knockout mouse models and lipidomics, we determined adipocyte-derived ceramide's contribution

to atherosclerotic plaque formation. Pharmacological HIF-1α inhibition could attenuate ceramide-induced atherosclerosis in *ApoE*$^{-/-}$ mice. It's worth noting that the inhibitory effect of PX-478 on adipose HIF-1α is remarkable (Fig. S5A and S5B), but the inhibition effect is universal by intraperitoneal injection. Therefore, it cannot be ruled out that reduced expression of HIF-1α in other tissues participated in the anti-atherosclerotic effects of PX-478. In addition, due to the vital role of hypoxia signaling in growth and development, regulation of ceramide metabolism by adipose HIF-1α may responsible for aggravating atherosclerosis partially, it is possible that other mechanisms are involved in the pro-atherosclerotic effects of adipose HIF-1α. Thus, the selective inhibitory effect of adipose HIF-1α can be used as a good strategy for atherosclerosis and exploring an adipose targeted drug delivery system will raise the security and practicability in clinical treatment. Taken together, our study identifies an important role for adipocyte HIF-1α in regulating lipid metabolism in atherosclerosis and provides a rationale for using HIF-1α specific inhibitor PX-478, as an adjunctive medical therapy, combined with current therapies to reduce the risk of atherosclerosis.

5. Conclusions

Reducing ceramide levels is a good strategy to ameliorate many metabolic disorders. This study partially clarifies the role of adipose-derived ceramide in the onset of atherosclerosis and provides a new strategy and drug candidate for the treatment of atherosclerosis. Adipocyte HIF-1α could be an effective target for treatment of metabolic dysregulation, and HIF-1α specific inhibitor PX-478 could exert metabolic benefits on atherosclerosis through inhibiting HIF-1α.

Acknowledgments

This work was supported by the National Key Research and Development Program of China (2018YFA0800700 and 2018YFC1003900) and the National Natural Science Foundation of China (Nos. 91857115, 31925021, 82022028 and 81921001).

Author contributions

Pengcheng Wang, Guangyi Zeng, Yu Yan, Song-yang Zhang, Yongqiang Dong, Yangming Zhang, Xingzhong Zhang, Huiying Liu and Zhipeng Zhang performed the experiments and analyzed the data. Yanli Pang and Changtao Jiang designed the study. Pengcheng Wang, Guangyi Zeng, Changtao Jiang and Yanli Pang wrote the manuscript. Pengcheng Wang and Guangyi Zeng contributed equally to this work. All authors edited the manuscript and approved the final manuscript.

Conflicts of interest

The authors declare no conflict of interest.

Appendix A. Supporting information

Supporting data to this article can be found online at https://doi.org/10.1016/j.apsb.2021.10.001.

References

1. Bittencourt MS. Beyond the stenosis paradigm: atherosclerosis burden on a risk prediction score for suspected chronic CAD. *JACC Cardiovasc Imaging* 2021;**14**:451−3.
2. Benjamin EJ, Muntner P, Alonso A, Bittencourt MS, Callaway CW, Carson AP, et al. Heart disease and stroke statistics—2019 update: a report from the american heart association. *Circulation* 2019;**139**:e56−528.
3. Tyrrell DJ, Goldstein DR. Ageing and atherosclerosis: vascular intrinsic and extrinsic factors and potential role of IL-6. *Nat Rev Cardiol* 2021;**18**:58−68.
4. Csige I, Ujvarosy D, Szabo Z, Lorincz I, Paragh G, Harangi M, et al. The impact of obesity on the cardiovascular system. *J Diabetes Res* 2018;**2018**:3407306.
5. Neeland IJ, Poirier P, Despres JP. Cardiovascular and metabolic heterogeneity of obesity: clinical challenges and implications for management. *Circulation* 2018;**137**:1391−406.
6. Atawia RT, Bunch KL, Toque HA, Caldwell RB, Caldwell RW. Mechanisms of obesity-induced metabolic and vascular dysfunctions. *Front Biosci (Landmark Ed)* 2019;**24**:890−934.
7. Hammarstedt A, Gogg S, Hedjazifar S, Nerstedt A, Smith U. Impaired adipogenesis and dysfunctional adipose tissue in human hypertrophic obesity. *Physiol Rev* 2018;**98**:1911−41.
8. Kita S, Maeda N, Shimomura I. Interorgan communication by exosomes, adipose tissue, and adiponectin in metabolic syndrome. *J Clin Invest* 2019;**129**:4041−9.
9. Neeland IJ, Yokoo T, Leinhard OD, Lavie CJ. 21st Century advances in multimodality imaging of obesity for care of the cardiovascular patient. *JACC Cardiovasc Imaging* 2021;**14**:482−94.
10. Kobiyama K, Ley K. Atherosclerosis. *Circ Res* 2018;**123**:1118−20.
11. Stower H. A shift in cholesterol geography. *Nat Med* 2020;**26**:1331.
12. Sun K, Tordjman J, Clement K, Scherer PE. Fibrosis and adipose tissue dysfunction. *Cell Metab* 2013;**18**:470−7.
13. Fuster JJ, Ouchi N, Gokce N, Walsh K. Obesity-induced changes in adipose tissue microenvironment and their impact on cardiovascular disease. *Circ Res* 2016;**118**:1786−807.
14. Bhupathiraju SN, Hu FB. Epidemiology of obesity and diabetes and their cardiovascular complications. *Circ Res* 2016;**118**:1723−35.
15. Kang JG, Sung HJ, Amar MJ, Pryor M, Remaley AT, Allen MD, et al. Low ambient oxygen prevents atherosclerosis. *J Mol Med (Berl)* 2016;**94**:277−86.
16. Seo JB, Riopel M, Cabrales P, Huh JY, Bandyopadhyay GK, Andreyev AY, et al. Knockdown of *Ant2* reduces adipocyte hypoxia and improves insulin resistance in obesity. *Nat Metab* 2019;**1**:86−97.
17. Choudhry H, Harris AL. Advances in hypoxia-inducible factor biology. *Cell Metab* 2018;**27**:281−98.
18. Wang K, Ding R, Ha Y, Jia Y, Liao X, Wang S, et al. Hypoxia-stressed cardiomyocytes promote early cardiac differentiation of cardiac stem cells through HIF-1alpha/Jagged1/Notch1 signaling. *Acta Pharm Sin B* 2018;**8**:795−804.
19. Watts ER, Walmsley SR. Inflammation and hypoxia: HIF and PHD isoform selectivity. *Trends Mol Med* 2019;**25**:33−46.
20. Downes NL, Laham-Karam N, Kaikkonen MU, Yla-Herttuala S. Differential but complementary HIF1alpha and HIF2alpha transcriptional regulation. *Mol Ther* 2018;**26**:1735−45.
21. Jun JC, Devera R, Unnikrishnan D, Shin MK, Bevans-Fonti S, Yao Q, et al. Adipose HIF-1alpha causes obesity by suppressing brown adipose tissue thermogenesis. *J Mol Med (Berl)* 2017;**95**:287−97.
22. Halberg N, Khan T, Trujillo ME, Wernstedt-Asterholm I, Attie AD, Sherwani S, et al. Hypoxia-inducible factor 1alpha induces fibrosis and insulin resistance in white adipose tissue. *Mol Cell Biol* 2009;**29**:4467−83.
23. Sun K, Halberg N, Khan M, Magalang UJ, Scherer PE. Selective inhibition of hypoxia-inducible factor 1alpha ameliorates adipose tissue dysfunction. *Mol Cell Biol* 2013;**33**:904−17.
24. Kasivisvanathan V, Shalhoub J, Lim CS, Shepherd AC, Thapar A, Davies AH. Hypoxia-inducible factor-1 in arterial disease—a putative therapeutic target. *Curr Vasc Pharmacol* 2011;**9**:333−49.

25. Jiang C, Qu A, Matsubara T, Chanturiya T, Jou W, Gavrilova O, et al. Disruption of hypoxia-inducible factor 1 in adipocytes improves insulin sensitivity and decreases adiposity in high-fat diet-fed mice. *Diebetes* 2011;**60**:2484−95.
26. Sasset L, Zhang Y, Dunn TM, Di Lorenzo A. Sphingolipid *de novo* biosynthesis: a rheostat of cardiovascular homeostasis. *Trends Endocrinol Metab* 2016;**27**:807−19.
27. Pagadala M, Kasumov T, McCullough AJ, Zein NN, Kirwan JP. Role of ceramides in nonalcoholic fatty liver disease. *Trends Endocrinol Metab* 2012;**23**:365−71.
28. Chaurasia B, Summers SA. Ceramides−lipotoxic inducers of metabolic disorders. *Trends Endocrinol Metab* 2015;**26**:538−50.
29. Neeland IJ, Singh S, McGuire DK, Vega GL, Roddy T, Reilly DF, et al. Relation of plasma ceramides to visceral adiposity, insulin resistance and the development of type 2 diabetes mellitus: the dallas heart study. *Diabetologia* 2018;**61**:2570−9.
30. Summers SA, Chaurasia B, Holland WL. Metabolic messengers: ceramides. *Nat Metab* 2019;**1**:1051−8.
31. Gertow J, Kjellqvist S, Stahlman M, Cheung L, Gottfries J, Werngren O, et al. Ceramides are associated with inflammatory processes in human mediastinal adipose tissue. *Nutr Metab Cardiovasc Dis* 2014;**24**:124−31.
32. Pavoine C, Pecker F. Sphingomyelinases: their regulation and roles in cardiovascular pathophysiology. *Cardiovasc Res* 2009;**82**:175−83.
33. Shamseddine AA, Airola MV, Hannun YA. Roles and regulation of neutral sphingomyelinase-2 in cellular and pathological processes. *Adv Biol Regul* 2015;**57**:24−41.
34. Czarny M, Schnitzer JE. Neutral sphingomyelinase inhibitor scyphostatin prevents and ceramide mimics mechanotransduction in vascular endothelium. *Am J Physiol Heart Circ Physiol* 2004;**287**:H1344−52.
35. Auge N, Maupas-Schwalm F, Elbaz M, Thiers JC, Waysbort A, Itohara S, et al. Role for matrix metalloproteinase-2 in oxidized low-density lipoprotein-induced activation of the sphingomyelin/ceramide pathway and smooth muscle cell proliferation. *Circulation* 2004;**110**:571−8.
36. Lallemand T, Rouahi M, Swiader A, Grazide MH, Geoffre N, Alayrac P, et al. nSMase2 (type 2-neutral sphingomyelinase) deficiency or inhibition by GW4869 reduces inflammation and atherosclerosis in *Apoe*$^{-/-}$ mice. *Arterioscler Thromb Vasc Biol* 2018;**38**:1479−92.
37. Canals D, Perry DM, Jenkins RW, Hannun YA. Drug targeting of sphingolipid metabolism: sphingomyelinases and ceramidases. *Br J Pharmacol* 2011;**163**:694−712.
38. Qin J, Berdyshev E, Poirer C, Schwartz NB, Dawson G. Neutral sphingomyelinase 2 deficiency increases hyaluronan synthesis by up-regulation of hyaluronan synthase 2 through decreased ceramide production and activation of Akt. *J Biol Chem* 2012;**287**:13620−32.
39. Kim WY, Safran M, Buckley MR, Ebert BL, Glickman J, Bosenberg M, et al. Failure to prolyl hydroxylate hypoxia-inducible factor alpha phenocopies VHL inactivation *in vivo*. *EMBO J* 2006;**25**:4650−62.
40. Xue X, Ramakrishnan S, Anderson E, Taylor M, Zimmermann EM, Spence JR, et al. Endothelial PAS domain protein 1 activates the inflammatory response in the intestinal epithelium to promote colitis in mice. *Gastroenterology* 2013;**145**:831−41.
41. Zhang X, Zhang Y, Wang P, Zhang SY, Dong Y, Zeng G, et al. Adipocyte hypoxia-inducible factor 2alpha suppresses atherosclerosis by promoting adipose ceramide catabolism. *Cell Metab* 2019;**30**:937−951 e935.
42. Li L, Shi L, Yang S, Yan R, Zhang D, Yang J, et al. SIRT7 is a histone desuccinylase that functionally links to chromatin compaction and genome stability. *Nat Commun* 2016;**20**:12235.
43. Wolf D, Ley K. Immunity and inflammation in atherosclerosis. *Circ Res* 2019;**124**:315−27.
44. Lawler PR, Bhatt DL, Godoy LC, Luscher TF, Bonow RO, Verma S, et al. Targeting cardiovascular inflammation: next steps in clinical translation. *Eur Heart J* 2021;**42**:113−31.
45. Welsh S, Williams R, Kirkpatrick L, Paine-Murrieta G, Powis G. Antitumor activity and pharmacodynamic properties of PX-478, an inhibitor of hypoxia-inducible factor-1α. *Mol Cancer Ther* 2004;**3**:233−44.
46. Després JP, Carpentier AC, Tchernof A, Neeland IJ, Poirier P. Management of obesity in cardiovascular practice: JACC focus seminar. *J Am Coll Cardiol* 2021;**78**:513−31.
47. Nakayama T, Kurobe H, Sugasawa N, Kinoshita H, Higashida M, Matsuoka Y, et al. Role of macrophage-derived hypoxia-inducible factor (HIF)-1alpha as a mediator of vascular remodelling. *Cardiovasc Res* 2013;**99**:705−15.
48. Rosso C, Kazankov K, Younes R, Esmaili S, Marietti M, Sacco M, et al. Crosstalk between adipose tissue insulin resistance and liver macrophages in non-alcoholic fatty liver disease. *J Hepatol* 2019;**71**:1012−21.
49. Lee YS, Kim JW, Osborne O, Oh DY, Sasik R, Schenk S, et al. Increased adipocyte O_2 consumption triggers HIF-1alpha, causing inflammation and insulin resistance in obesity. *Cell* 2014;**157**:1339−52.
50. Maceyka M, Spiegel S. Sphingolipid metabolites in inflammatory disease. *Nature* 2014;**510**:58−67.
51. Choi RH, Tatum SM, Symons JD, Summers SA, Holland WL. Ceramides and other sphingolipids as drivers of cardiovascular disease. *Nat Rev Cardiol* 2021;**18**:701−11.
52. Jiang XC, Paultre F, Pearson TA, Reed RG, Francis CK, Lin M, et al. Plasma sphingomyelin level as a risk factor for coronary artery disease. *Arterioscler Thromb Vasc Biol* 2000;**20**:2614−8.
53. Meikle PJ, Summers SA. Sphingolipids and phospholipids in insulin resistance and related metabolic disorders. *Nat Rev Endocrinol* 2017;**13**:79−91.
54. Fan Y, Shi F, Liu J, Dong J, Bui HH, Peake DA, et al. Selective reduction in the sphingomyelin content of atherogenic lipoproteins inhibits their retention in murine aortas and the subsequent development of atherosclerosis. *Arterioscler Thromb Vasc Biol* 2010;**30**:2114−20.
55. Xia JY, Holland WL, Kusminski CM, Sun K, Sharma AX, Pearson MJ, et al. Targeted induction of ceramide degradation leads to improved systemic metabolism and reduced hepatic steatosis. *Cell Metab* 2015;**22**:266−78.
56. Xie C, Yagai T, Luo Y, Liang X, Chen T, Wang Q, et al. Activation of intestinal hypoxia-inducible factor 2alpha during obesity contributes to hepatic steatosis. *Nat Med* 2017;**23**:1298−308.
57. Cogolludo A, Moreno L, Frazziano G, Moral-Sanz J, Menendez C, Castaneda J, et al. Activation of neutral sphingomyelinase is involved in acute hypoxic pulmonary vasoconstriction. *Cardiovasc Res* 2009;**82**:296−302.
58. Moreno L, Moral-Sanz J, Morales-Cano D, Barreira B, Moreno E, Ferrarini A, et al. Ceramide mediates acute oxygen sensing in vascular tissues. *Antioxid Redox Signal* 2014;**20**:1−14.
59. Boon J, Hoy AJ, Stark R, Brown RD, Meex RC, Henstridge DC, et al. Ceramides contained in LDL are elevated in type 2 diabetes and promote inflammation and skeletal muscle insulin resistance. *Diabetes* 2013;**62**:401−10.
60. Summers SA. Could ceramides become the new cholesterol?. *Cell Metab* 2018;**27**:276−80.
61. Chiang JY. Bile acids: regulation of synthesis. *J Lipid Res* 2009;**50**:1955−66.
62. Koh MY, Spivak-Kroizman T, Venturini S, Welsh S, Williams RR, Kirkpatrick DL, et al. Molecular mechanisms for the activity of PX-478, an antitumor inhibitor of the hypoxia-inducible factor-1alpha. *Mol Cancer Ther* 2008;**7**:90−100.